PHYSICAL REVIEW B **93**, 174116 (2016)

Time-resolved photoluminescence spectroscopy of $\mathrm{Nb}_{\mathrm{Nb}}^{4+}$ and O^- polarons in LiNbO_3 single crystals

T. Kämpfe,[*] A. Haußmann, and L. M. Eng
Institut für Angewandte Photophysik, Technische Universität Dresden, 01069 Dresden, Germany
and Center for Advancing Electronics Dresden (cfaed), 01062 Dresden, Germany

P. Reichenbach and A. Thiessen
Institut für Angewandte Photophysik, Technische Universität Dresden, 01069 Dresden, Germany

T. Woike
Institut für Strukturphysik, Technische Universität Dresden, 01069 Dresden, Germany

R. Steudtner
Institut für Ressourcenökologie, Helmholtz-Zentrum Dresden-Rossendorf, 01328 Dresden, Germany

(Received 14 January 2016; revised manuscript received 5 April 2016; published 25 May 2016)

We probe here the optical relaxation properties of Mg-doped wide-band-gap LiNbO_3 single crystals with both a high spectral and temporal resolution at cryogenic temperatures. Surprisingly, we observe the photoluminescence to decay in a two-step process: a fast relaxation and a slower one centered around an energy $E_{\max} = 2.62 \pm 0.05$ eV. Both decays fit well to the stretched-exponential behavior. Moreover, we are able to associate these energies to the recombination of light-induced $\mathrm{Nb}_{\mathrm{Nb}}^{4+}$ and O^- small polarons. Also, we checked the stability of our findings by using LiNbO_3 single crystals that show *on-purpose* modified radiative recombination processes, i.e., with a Mg doping both above and below the optical damage resistance threshold, as well as with different poling histories of inverted domains.

DOI: 10.1103/PhysRevB.93.174116

I. INTRODUCTION

Lithium niobate (LiNbO_3) is an intensively applied optical material well known for its special acousto-optical, electro-optical, photorefractive, birefringent, nonlinear optical, and ferroelectric properties. Most common applications incorporate (thin-film) LiNbO_3 into Mach-Zehnder and surface acoustic wave modulators. The optical endurance and robustness of LiNbO_3 also make this material to be favorable for exploring modern-type broad-band storage devices such as holographic memories [1–3].

LiNbO_3 exhibits an excellent optical transmittance over a broad spectral wavelength range, providing a high optical damage resistance threshold (ODRT). Moreover, dopants such as Mg^{2+}, Zn^{2+}, and In^{3+} may significantly increase the ODRT both for visible and near-infrared wavelengths [4,5], which is especially beneficial to any nonlinear optical application. Mg-doped LiNbO_3 (Mg:LiNbO_3), therefore, is a very suitable material when it comes to applications involving optical parametric amplification and frequency doubling, e.g., via quasi-phase matching.

Upon ultrashort laser pulse excitation, higher order absorption processes are invoked in LiNbO_3 [6–8]. Generally, excited charge carriers distribute over the conduction and valence band (CB, VB) and then relax into intergap states that concurrently may increase the absorption cross section. However, in order to increase and engineer the power threshold beyond the natural ODRT in these materials, it is necessary to quantify and understand all the occurring optical transition processes with respect to both their temporal and spectral behavior. For such an analysis, time-resolved absorption (TRA) spectroscopy most preferentially has been applied, stating, for instance, that the decay of intergap states follows the famous Kohlrausch-Williams-Watts (KWW) relation [9]. Photoluminescence (PL) spectroscopy, on the contrary, has rarely been applied, although being an as-powerful method as compared to TRA. From the PL photon energy, we can directly deduce the energy levels of the acceptor intergap states. This example shows that PL measurements may provide valuable complementary insight that is not possible with TRA.

The most frequently discussed intergap states in LiNbO_3 are bound and free small polarons [10]. In LiNbO_3 four intrinsic polaronic centers were reported that might be taken into account to explain the PL as discussed here: three *electron* polarons and one *hole* polaron. More precisely, these are the following ones:

(i) a free small polaron $\mathrm{Nb}_{\mathrm{Nb}}^{4+}$;
(ii) a bound small polaron $\mathrm{Nb}_{\mathrm{Li}}^{4+}$;
(iii) a bound bipolaron $\mathrm{Nb}_{\mathrm{Li}}^{4+}$:$\mathrm{Nb}_{\mathrm{Nb}}^{4+}$; and
(iv) a free hole polaron O^-.

The energy levels of the electron polarons were investigated by TRA [11], while up to now the energy levels of the hole polarons are unknown. Assuming a band gap of 4 eV and energy levels of bound and free electron polarons of about 1 and 1.5 eV below the CB, we can deduce the energy of the hole polaron above VB from the PL energy. The here-reported PL energy of 2.6 eV thus would yield an energy level of the hole polaron of about 0.9 eV above VB. The comparison of TRA and time-resolved photoelectron spectroscopy (TRPLS) in LiNbO_3 is depicted in Fig. 1.

---

[*] thomas.kaempfe@iapp.de

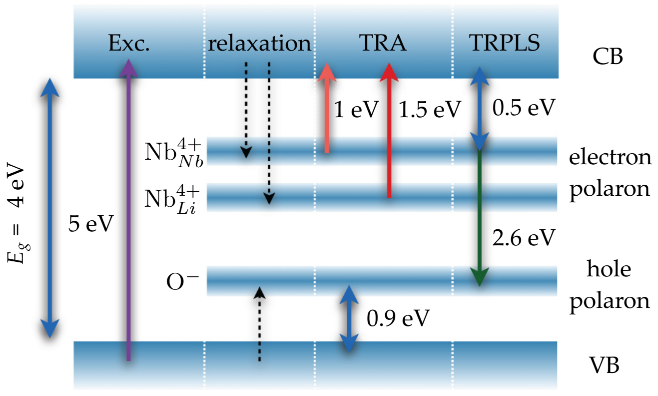

FIG. 1. Comparison of time-resolved absorption (TRA) and PL spectroscopy (TRPLS) in $LiNbO_3$.

It has been shown that intergap states can form an ensemble of emitters with distributed decay rates, e.g., in distorted materials. The effective number of involved excited states may then be deduced via Laplace transformation of the decay-rate distribution [12] and one obtains

$$n(t) = n_0 \exp[-(t/\tau)^\beta], \tag{1}$$

with n_0 being the number of excited charge carriers, τ the total decay time, and β the stretch parameter that may vary between 0 and 1. β qualitatively expresses the underlying distribution of decay rates: a small β value thus represents a broad rate distribution, while a β close to 1 defines a narrow and discrete distribution. Even though Eq. (1) was derived from macroscopic phenomenological findings, its application to TRA data was shown to be very successful. The number of excited charge carriers in intergap states depends proportionally on the absorption for sub-band-gap illumination. In TRA measurements stretched-exponential decays were consistently reported for $LiNbO_3$ [13–17].

As radiative and nonradiative decay channels may superpose at room temperature, it is favorable to perform PL experiments at cryogenic conditions, as the nonradiative recombination processes are completely inhibited, resulting in a dramatically increased PL (Fig. 2). Assuming negligible nonradiative decays and the measured PL to stem solely from these intergap states, the PL has to fulfill $I(t) = -\partial_t n(t)/n_0$, revealing the response to decay in the following way:

$$I(t) = I_0\, t^{\beta-1} \exp[-(t/\tau)^\beta], \tag{2}$$

with $I_0 = \beta\,\tau^{-\beta}$, and τ being the generalized decay time.

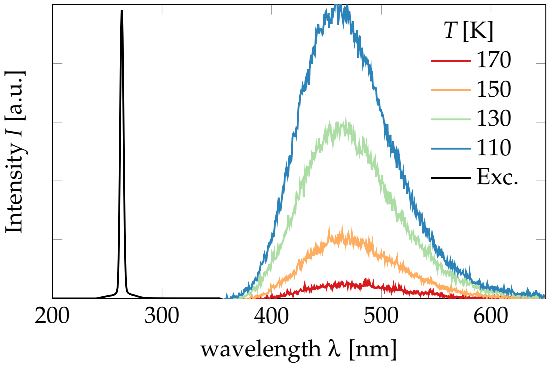

FIG. 2. Corrected steady-state PL spectrum in LNO7 for different cryogenic temperatures T for the given excitation laser spectrum denoted as Exc.

In this publication, we investigate the PL decay in Mg:$LiNbO_3$ upon super-band-gap illumination with spectral resolution and recording over several orders of magnitude in both time and intensity. We find a stretched-exponential temporal decay [see Eq. (2)] to fit our data as well, similar to TRA measurements. In addition, our spectral PL analysis allows associating these energies to relaxation channels and recombination processes from intergap states in sc-$LiNbO_3$. Therefore, we can introduce time-resolved PL measurements as a general way to further understand photorelaxation properties in $LiNbO_3$, which appears to be necessary for future ODRT research.

The luminescent properties of nondoped $LiNbO_3$ have previously been investigated by electron beam, x-ray, photo- and thermostimulated studies [18,19], proposing a band scheme that contains several intergap states. Doping congruent $LiNbO_3$ with the lanthanide Er^{3+} yields a by-magnitudes brighter luminescence. The lanthanide ions can act as a local probe and, thus, recording the PL energy shifts, can reveal the local crystal field [20,21]. Also, time-resolved PL measurements were conducted for highly Mg-doped sc-$LiNbO_3$ spanning a time frame between 200 ns and 1 μs [22], however, without delivering any spectral differentiation. When summarizing the PL reports in as-grown $LiNbO_3$, two main fluorescence energies were observed: one around 2.6 eV in the visible range and another around 1.5 eV in the near-IR range [23,24].

PL was not only observed upon super-band-gap excitation, but also upon ultrafast multiphoton excitation in Mg:$LiNbO_3$ [7]. The reported PL showed an onset close to the ODRT that resulted even in a domain contrast; as-grown samples, for instance, showed a stronger PL as compared to singly inverted domains. The PL contrast was observed to decrease under thermal annealing with an activation energy of about 1 eV [8]. The deduced threshold temperatures agreed well with previous reports [25], concluding that the PL must be driven by the specific defect concentration and formation.

II. SETUP AND MATERIALS

The samples used for this study are z-cut, congruent $LiNbO_3$ single crystals of a $d = 500\ \mu$m thickness purchased from United Crystals, Inc., and Union Optics, respectively, with either a 3 mol % Mg:$LiNbO_3$ (LNO3) or a 7 mol % Mg:$LiNbO_3$ (LNO7) Mg content. LNO3 and LNO7 thus constitute samples well below and well above the ODRT, respectively. LNO3 and LNO7 were used both as grown and in a singly inverted domain configuration; the latter was achieved by applying an electrical field of 4 kV/mm using electrolytic contacts as described in [7,8].

TRPLS was carried out on all these samples under a 45° incident angle using $t_{\mathrm{FWHM}} = 4$ ns excitation pulses at a $\lambda_{\mathrm{exc}} = 266$ nm from a Q-switched cascaded frequency-doubled Nd:YAG laser (Continuum Minilite). The average incident UV power density reached 40 GW/m^2 with a relative pulse-energy standard deviation of <2%. PL was

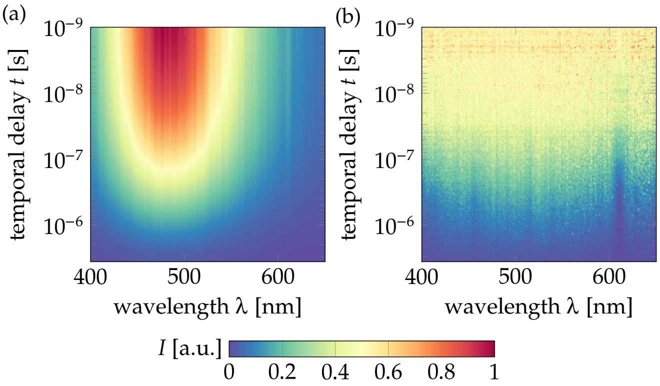

FIG. 3. Time-resolved PL decay $I(t,\lambda)$ in as-grown LNO7 (a) and normalized decay $I(t,\lambda)/I(t=0,\lambda)$ (b).

recorded perpendicular to the incident beam in back-reflection geometry using a quartz fiber that was mounted onto a spectrometer/ICCD setup from Horiba-Jobin-Yvon (Horiba iHR 550). Standard spectrometer settings comprise a 2-μm entrance slit width and an internal MCP amplification factor of 128. The temporal PL evolution was detected with an exponential increase in time delays between 1 ms and 16 ms and a minimal integration period of 2 ns. In each time step, the recorded gated spectra of 50 individual pulses were averaged. The sample was mounted within a liquid nitrogen cryostat and cooled down to 100–200 K in dry nitrogen gas at atmospheric pressure.

III. RESULTS

A. As-grown LNO7

We start by discussing the results of the as-grown 7 mol % Mg:LiNbO$_3$ (LNO7). Figure 2 displays the well-known steady-state (cw) PL spectra for different cryogenic temperatures, while Fig. 3(a) reports the TRPLS of the same sample recorded at $T = 150$ K over the spectral and temporal range from 400 nm to 650 nm and 10^{-9} s to 3×10^{-6} s, respectively. cw and TRPL spectra are pretty identical over the whole wavelength range, exhibiting also equal decay rates as is typical to a single radiative transition process. Assuming an achromatic PL decay of Gaussian distribution allows transforming Fig. 3(a) into the normalized plot, as shown in Fig. 3(b), with a center energy and width of $E_1^{\max} = 2.62 \pm 0.05$ eV and $w_1 = 0.30 \pm 0.03$ eV, respectively.

Figure 4(a) illustrates these same data but recorded for up to 16-ms delay times. Surprisingly, a second transition peak pops up at around 475 nm, as best seen for $t > 10^{-3}$. Also, this peak follows a stretched-exponential behavior but is clearly separated from the "ordinary" radiative decay (as reported above). This new peak slightly shifts to $E_2^{\max} = 2.65 \pm 0.01$ eV while also becoming narrower in width by $w_2 = 0.14 \pm 0.01$ eV [Fig. 4(c)]. The normalized PL decay [Fig. 4(d)] hence may be best fitted to the following superposition of two stretched-exponential decays:

$$I(t) = \sum_{i=1,2} I_i\, t^{\,\beta_i - 1} \exp\left[-(t/\tau_i)^{\beta_i}\right]. \qquad (3)$$

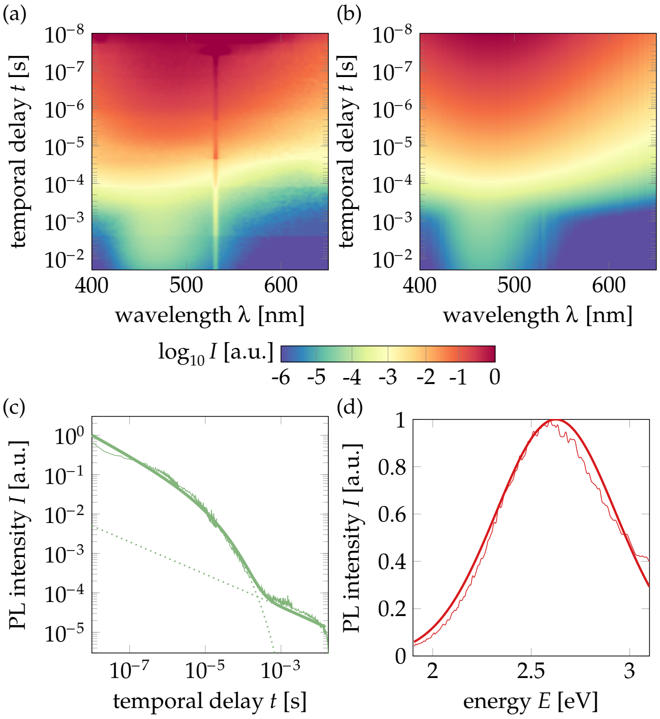

FIG. 4. Time-resolved PL decay in as-grown LNO7. (a) Raw TRPLS data, (b) corrected TRPLS data, (c) PL spectrum for $\lambda = 475$ nm, and (d) PL spectrum for a delay time $t = 2 \times 10^{-8}$ s.

Fitting this distribution with Eq. (3) readily yields $\tau_1 = (12 \pm 2) \times 10^{-6}$ s and $\tau_2 = (1.1 \pm 0.5) \times 10^{0}$ s, as well as $\beta_1 = 0.48 \pm 0.07$ and $\beta_2 = 0.59 \pm 0.08$. The ratio of radiative strength between the two transitions measures

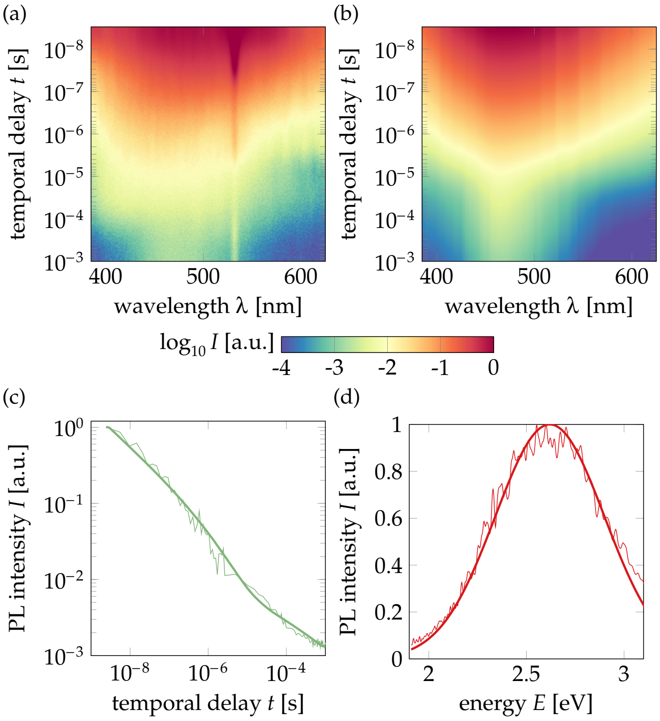

FIG. 5. Time-resolved PL decay in as-grown LNO3. (a) Raw TRPLS data, (b) corrected TRPLS data, (c) PL decay for $\lambda = 475$ nm, and (d) PL spectrum for a delay time $t = 2 \times 10^{-8}$ s.

TABLE I. Characteristic lifetimes $\tau_{1,2}$, stretched-exponential parameters $\beta_{1,2}$, the equivalent intensities $I_{1,2}^{\max}$, the mean energy $E^{\max}$, and width w for as-grown Mg:LiNbO$_3$ at $T = 150$ K.

c_{Mg} [mol %]	i	τ_i [s]	β_i	$I_i^{\max}$ [a.u.]	$E^{\max}$ [eV]	w [eV]
7	1	$(12 \pm 2) \times 10^{-6}$	0.48 ± 0.05	1	2.6 ± 0.1	0.30 ± 0.03
	2	$(1.1 \pm 0.2) \times 10^{0}$	0.59 ± 0.05	$(3.5 \pm 0.5) \times 10^{-2}$		
3	1	$(2.0 \pm 0.5) \times 10^{-6}$	0.52 ± 0.11	$(2.3 \pm 0.3) \times 10^{-3}$	2.6 ± 0.1	0.28 ± 0.03
	2	$(1.0 \pm 0.5) \times 10^{-2}$	0.70 ± 0.05	1		

$I_1/I_2 = 1 : (3.5 \pm 0.5) \times 10^{-2}$. Comparing the modeled results in Fig. 4(b) finally rationalizes our assumption of two independent decay processes to coexist in LNO7.

B. As-grown LNO3

As-grown 3 mol % Mg:LiNbO$_3$ (LNO3) shows a PL that is by 2 orders of magnitude weaker as compared to as-grown LNO7, as displayed in Fig. 5(a) for $T = 150$ K. The time delay was varied here from 3×10^{-8} s to 3×10^{-3} s. Applying Eq. (3) yields decay times $\tau_1 = (2.0 \pm 0.5) \times 10^{-6}$ s and $\tau_2 = (1.0 \pm 0.5) \times 10^{-2}$ s with $\beta_1 = 0.52 \pm 0.05$ and $\beta_2 = 0.70 \pm 0.05$, values that are pretty identical to the LNO7 sample. Nevertheless, the ratio of both transition intensities shows an inverted behavior as compared to LNO7 with $I_1/I_2 = (2.3 \pm 0.3) \times 10^{-3} : 1$. The central energy is $E^{\max} = 2.62 \pm 0.05$ eV with a width $w_1 = 0.28 \pm 0.03$ eV, which is very close to the findings in LNO7. For larger delay times t, a gradual blueshift and peak narrowing is observed. Table I finally summarizes these two transition processes in as-grown LNO3 and LNO7 samples by comparing all the relevant data, i.e., decay times, stretched-exponential parameters, intensities, center energies, and peak widths at $T = 150$ K.

C. Linearity

To exclude nonlinear temporal PL decay processes in Mg:LiNbO$_3$, e.g., associated with inhomogeneous population densities, the TRPL graphs were recorded at different pump intensities. As depicted in Fig. 6, the PL signal shows a linear dependence on incident power over almost 2 decades, which vastly excludes nonlinear processes to be accounted for in the present TRPL study too.

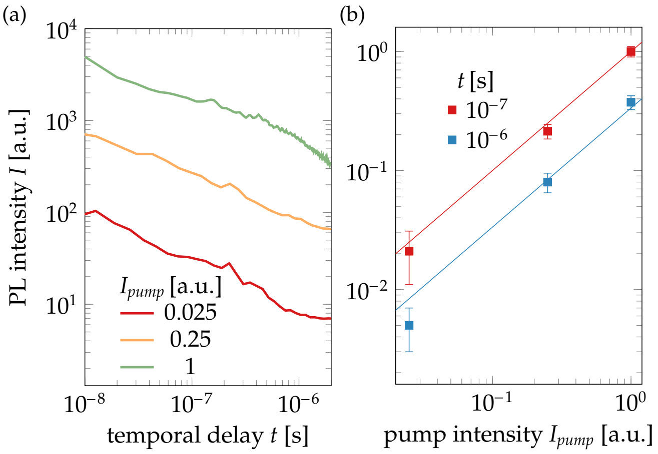

FIG. 6. (a) TRPLS graphs for different pump intensities. (b) A clear proportional dependence of the integrated PL for two representative delay times can be observed; thus, nonlinear relaxation processes can therefore be largely excluded.

D. Singly inverted LNO3 and LNO7

We now investigate the impact on TRPL of singly inverted domains in LNO3 and LNO7. As shown in Fig. 7, the PL decays faster in as-treated LiNbO$_3$ samples for both high and low Mg concentrations as compared to as-grown LiNbO$_3$. Since β is determined by the fast decaying processes at $t \ll \tau$, we record TRPL for up to 10^{-6} s [see Figs. 7(a) and 7(b)] and extract the stretched-exponential parameters as $\beta_1 = 0.23 \pm 0.03$ and $\beta_1 = 0.44 \pm 0.04$ for LNO3 and LNO7, respectively. These values are much smaller when compared to as-grown LiNbO$_3$ (see Table II as a summary). Moreover, the smaller β for singly inverted LiNbO$_3$ samples clearly hints towards a larger variation of decay rates after poling, resulting in a reduced integrated PL intensity. Note, however, that no alterations in the spectral shape between any of these samples were observed.

E. Temperature dependence

As displayed in Fig. 2 the steady-state PL shows a strong intensity increase upon cooling. We, therefore, can assume the transitions to be thermally activated. Such thermally activated radiative recombination processes follow an Arrhenius-like behavior described as follows:

$$\tau(T) = Z^{-1} \exp\left[E_a/(k_B T)\right], \qquad (4)$$

with k_B the Boltzmann constant and Z the frequency factor. Hereby, the frequency factor can be understood as a rate or recombination coefficient. We thus inspected LNO7 samples by TRPL over the temperature range from 100 K to 200 K. Representative TRPL graphs are given in Fig. 8 for $T = 100$ K and 200 K, respectively. The experimental TRPLS graphs are compared to the optimally fitted graphs, taking into account the stretched-exponential decay with two transitions as given by Eq. (3). One can observe a strong decrease in the

TABLE II. PL decay parameters for different doping concentrations and preparations at $T = 130$ K.

Mg [mol %]	Preparation	β_1
3	As-grown	0.40 ± 0.05
	1 × poled	0.23 ± 0.03
7	As-grown	0.52 ± 0.07
	1 × poled	0.44 ± 0.04

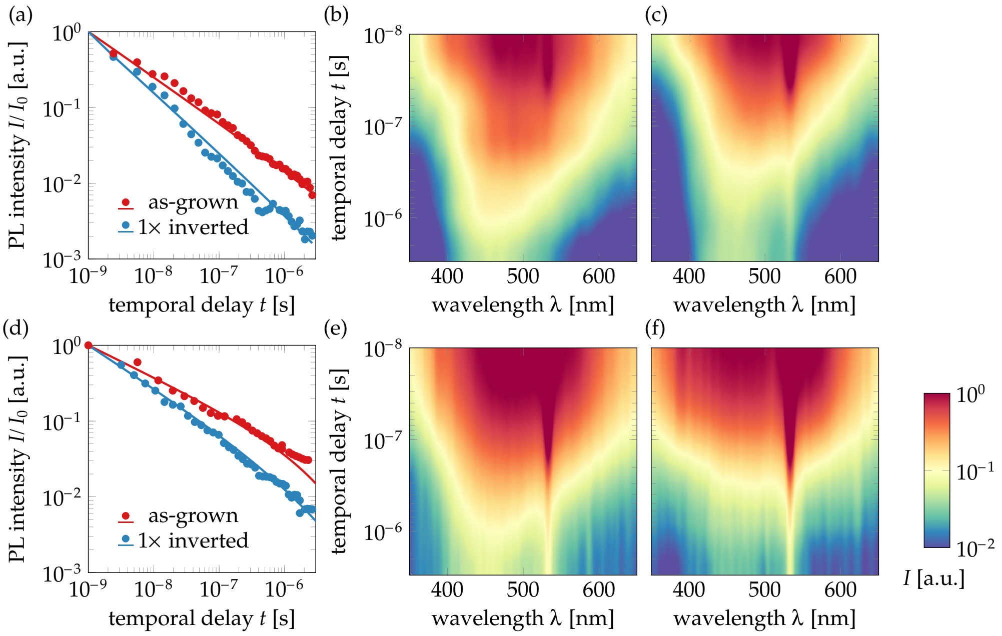

FIG. 7. PL decay in as-grown and singly inverted LNO7 (a) PL decay in LNO3 (d) in LNO3. TRPLS graphs for LNO3 and LNO7: (b) as-grown and (c) singly inverted in the case of LNO7; (d) as-grown and (e) singly inverted in the case of LNO3.

second transition for lower temperatures. The normalized PL at $\lambda = 475$ nm is plotted in Fig. 9 for the given temperature range. We can see a strong change in the overall signal. The PL intensity was fitted again, assuming two stretched-exponential decays. By plotting the fitted decay times $\tau_{1,2}$ by means of an Arrhenius plot as is done in Fig. 10, we can observe a thermally activated process for temperatures above 150 K and 140 K, respectively. For lower temperatures a much smaller dependence on temperature was observed. For the higher temperatures the extractable activation energies are $E_a^{(1)} = (140 \pm 10)$ meV and $E_a^{(2)} = (110 \pm 10)$ meV. For lower temperatures we did not apply the model of a thermally excited process, as such a drastic change in slope in an Arrhenius plot does suggest the decay time to be basically determined by a temperature-independent process. The extracted activation energy is in good agreement with previously reported activation energies in the case of 6.5 mol % Mg:LiNbO$_3$, which is in detail given in Table III. The stretch parameters $\beta_{1,2}$ undergo a strong alteration over the investigated temperature range (Fig. 11). Both β_1 and β_2 increase towards lower temperatures, which conclusively suggests that for lower

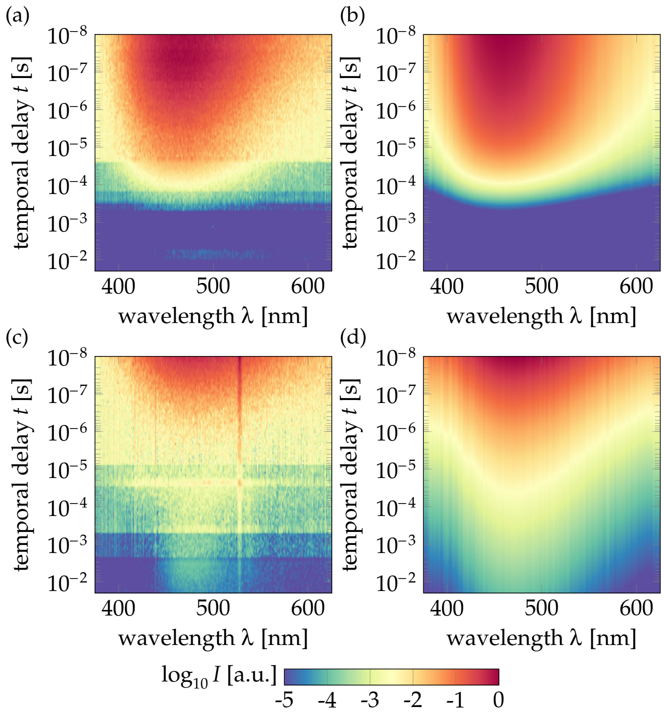

FIG. 8. Normalized TRPLS graphs for 7 mol % Mg:LiNbO$_3$ for different temperatures $T = 200$ K (a) and $T = 100$ K (c). The corrected TRPLS graph is given in (b), (d), respectively.

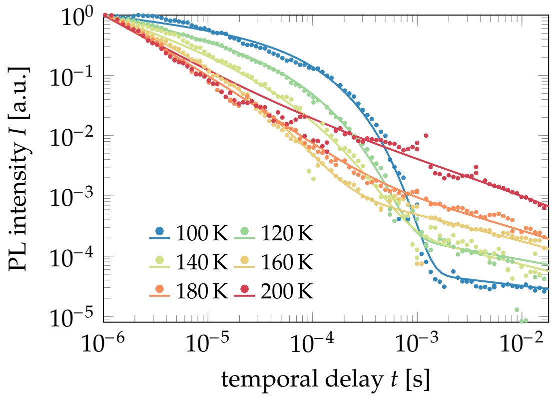

FIG. 9. TRPL curves at $\lambda = 475$ nm for a temperature range of 100 K to 200 K. Hereby, dots represent experimental data and lines the fitting curves according to Eq. (3).

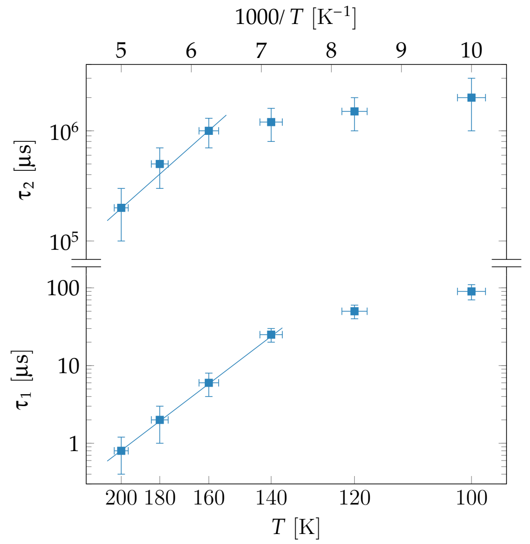

FIG. 10. Arrhenius plot of the characteristic lifetimes $\tau_{1,2}$ of the fast and slow decay versus temperature. Theoretical fit with $E_a^{(1)} = (140 \pm 10)$ meV and $E_a^{(2)} = (110 \pm 10)$ meV.

temperatures hopping transport appears to be an inappropriate description for the transport and recombination process, which is in good agreement with the finding of a transition to a nonactivated recombination process. The absolute strength of both transitions $I_{1,2}$ drastically changes over the temperature range. For higher temperatures the slower transition is mainly determining the overall relaxation, whereas for lower temperatures the faster transition determines the relaxation (Fig. 12).

IV. DISCUSSION

Our combined spectral and temporal analysis allows us to exclude recombination processes that might be invoked in $LiNbO_3$ upon illumination. Mainly, this refers to radiative relaxations following a mono- or biexponential decay, as well as mechanisms resulting in PL at different photon energies.

$LiNbO_3$ is known to incorporate impurities even for a nominally nondoped, pure stoichiometry. In congruent $LiNbO_3$ we most commonly find $Fe^{2+/3+}$ ions with a concentration of typically 5 ppm [4]. However, neither the impurity concentration nor the PL spectra reported for highly Fe-doped $LiNbO_3$ can explain the PL data that we report here, since the center PL energy was observed at $E \approx 1.4$ eV in Fe:$LiNbO_3$ [24] and undergoes a monoexponential decay.

Notably, we can exclude the presence of Nb_{Li}^{4+}:Nb_{Nb}^{4+} bipolarons, which have only been observed in reduced $LiNbO_3$. Upon Mg doping Mg_{Li}^{2+} defects are formed, reducing the number of Nb_{Li}^{4+} antisites, which in turn dramatically affects the reported ODRT, as the concentration of light-induced Nb_{Li}^{4+} bound small polarons reduces [27]. An increase in PL by 2 orders of magnitude was reported above ODRT [22]. A possible explanation is the formation of Mg_{Nb}^{2+} defects at these conditions. It is very likely that the induced disorder results in the increase in PL. Moreover, phonon coupling was readily shown to depend on Mg doping concentration and shows a steplike increase at the ODRT [28].

TABLE III. Comparison of time-resolved PL and absorption at different wavelengths λ_{abs} in above-threshold Mg:$LiNbO_3$.

Mg [mol %]	λ_{abs} [nm]	$E_a^{(1)}$ [eV]	Z [Hz]	Ref.
6.5	488	0.16 ± 0.05	$(3.0 \pm 1.0) \times 10^8$	[26]
6.5	405	0.14 ± 0.05	$(1.0 \pm 0.5) \times 10^8$	[26]
7		0.14 ± 0.02	$(3.0 \pm 0.5) \times 10^8$	Here

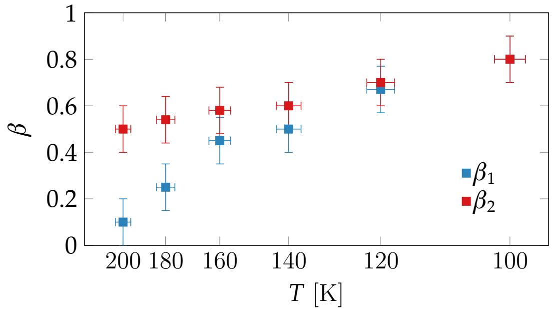

FIG. 11. Temperature dependence of the stretch parameters β_i for fast ($i = 1$) and slow ($i = 2$) transitions.

The observed nonexponential relaxation dynamics are in good agreement with theoretical expectations for the localized carrier dynamics in oxide crystals, even without structural or energetic disorder. A thermally activated diffusive hopping transport under trap saturation can result in stretched-exponential carrier concentrations [26,29]. Notably, in this context the hole polarons were treated as traps with free electron polarons being allowed to distribute homogeneously over the lattice. In our work here, the recorded PL in Mg:$LiNbO_3$ follows a stretched-exponential decay. Taking the emission energy of approximately 2.6 eV and the proposed energies of polaronic inter-band-gap energies in $LiNbO_3$ [11] into account, we conclude that only a polaronic recombination of the free electron polaron Nb_{Nb}^{4+} and the hole polaron O^- can fully explain our time-resolved PL spectra.

A two-step recombination process, as was apparent in the presented TRPL, has already been reported in reduced $LiNbO_3$ [30] by means of room-temperature TRA. It was associated to recombination processes of free and bound electron polarons. However, in our case, we can exclude bound polarons to be related to the slow recombination process, since

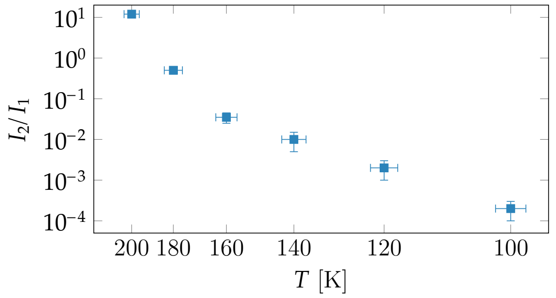

FIG. 12. Temperature dependence of the ratio of fast- (1) and slow- (2) transition PL intensities I_2/I_1.

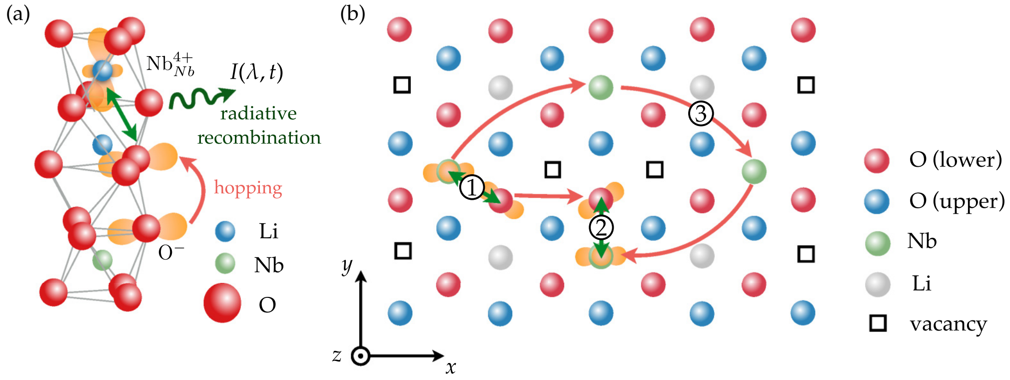

FIG. 13. (a) Schematic of radiative recombination of electron and hole polaron in $\mathrm{LiNbO_3}$ after hopping transport. (b) Different radiative recombination properties: ① single-step hopping recombination, and ② several-step recombination after several hopping steps ③.

no redshifted PL for longer time delays was observed. A two-step stretched-exponential decay was theoretically discussed as a result of the site-correlation effect in random walk Monte Carlo simulations [31]. In the case of site correlation the walk starts directly in the vicinity of the trap. As we assume the PL to be a result of a recombination of the electron and hole polaron formed upon light-induced electron-hole pair relaxation and one typically generates a large fraction of electron and hole polarons in direct vicinity, only a single to a few hopping events are required for recombination, resulting in the fast transition. Only a smaller fraction of generated electrons and holes are further separated before relaxation, resulting in trap saturation and hence the observed stretched-exponential decay. As a larger number of steps for recombination is required, it becomes increasingly less probable to recombine for lower temperatures. We can observe this behavior, which is depicted in Fig. 12. For low temperatures the PL is mainly governed by the fast transition, requiring only a small number of hopping events. The main idea of the radiative recombination process observed in our PL measurements is given in Fig. 13. A one-site hopping recombination gives a fast relaxation, which is understood in site correlation, whereas the slow relaxation can be attributed to trap saturation for few-to-many hopping events.

The difference in PL strength and decay characteristics of LNO3 and LNO7 can be attributed to the influence of $\mathrm{Mg}^{2+}_{\mathrm{Nb}}$ defects resulting in local distortions. Above ODRT, a significant amount of $\mathrm{Mg}^{2+}_{\mathrm{Nb}}$ centers are generated with a larger defect potential energy as $\mathrm{Mg}^{2+}_{\mathrm{Li}}$ [27]. Concurrently, the $\mathrm{Mg}^{2+}_{\mathrm{Nb}}$ centers give rise to larger perturbations of the local crystal field. This would explain the reduction of the stretch parameters upon ferroelectric poling, e.g., as a result of increased distortion. This corresponds to previously observed domain-specific multiphoton PL [8] and suggests an incomplete poling process, only to be completed upon thermal annealing.

For free small polarons in $\mathrm{LiNbO_3}$, E_p was reported to measure approximately 0.54 eV [11]. Assuming a harmonic oscillator potential, this results in a hopping transport activation energy $E_a = E_p/2$ of 0.27 eV, which is comparably larger than the observed thermal activation in this measurement. Nevertheless, the latter assumption is a simplified case and, hence, systematically overestimates the activation energy when compared to more realistic potential curves. The activation energies for polaron recombination reported here are in similar good agreement with electrical conductance measurements in ferroelectric domain walls in the investigated material [32]. Accordingly, for lower temperatures a decrease in the activation energy was observed [33]. For lower temperatures the transition times do show a much smaller increase upon cooling, which cannot be explained in the concept of thermal activation. A possible explanation of this phenomenon could be an increase in internal conversion.

V. CONCLUSION

In conclusion, we reported here measurements on the polaron PL in a special wide-band-gap oxide, Mg-doped $\mathrm{LiNbO_3}$, with both high spectral and temporal resolution. We obtained clear significance of two independent radiative relaxation components. The recorded temporal PL decay is a consequence of the light-induced hopping transport that finally results in the radiative recombination of free electron and hole polarons. We further obtain understanding for induced distortion upon ferroelectric poling, resulting in a change in radiative relaxation dynamics.

Moreover, we show that time-resolved photoluminescence spectroscopy (TRPLS) can be applied as a complementary method to time-resolved absorption (TRA). For doped $\mathrm{LiNbO_3}$, TRPLS provides a nondispensable method to quantify and optimize the optical damage resistance, as needed, for instance, in high-power applications, especially in nonlinear optics. As shown, the observed PL at $E = 2.6$ eV is an optimal reference tool to investigate the optical damage resistance.

ACKNOWLEDGMENTS

T.K., A.H., and L.M.E. acknowledge the Cluster of Excellence "Center of Advancing Electronics Dresden" for funding. P.R. thanks Deutsche Forschungsgemeinschaft/German Science Foundation (DFG) for funding via the DFG priority program 1237 and the European Social Fund (ESF) through the ESF-NFG "Mind Nano." A.H. appreciates funding via DFG Research Grant No. HA 418 6982/1-1.

[1] A. V. Ievlev, A. N. Morozovska, E. A. Eliseev, V. Y. Shur, and S. V. Kalinin, Nat. Commun. **5**, 4545 (2014).

[2] S. Odoulov, A. Shumelyuk, H. Badorreck, S. Nolte, K.-M. Voit, and M. Imlau, Nat. Commun. **6**, 5866 (2015).

[3] H. Brüning, V. Dieckmann, B. Schoke, K. M. Voit, M. Imlau, G. Corradi, and C. Merschjann, Opt. Express **20**, 13326 (2012).

[4] O. F. Schirmer, O. Thiemann, and M. Wöhlecke, J. Phys. Chem. Solids **52**, 185 (1991).

[5] T. R. Volk, V. I. Pryalkin, and N. M. Rubinina, Opt. Lett. **15**, 996 (1990).

[6] O. Beyer, D. Maxein, K. Buse, B. Sturman, H. T. Hsieh, and D. Psaltis, Phys. Rev. E **71**, 056603 (2005).

[7] P. Reichenbach, T. Kämpfe, A. Thiessen, M. Schröder, A. Haußmann, T. Woike, and L. M. Eng, J. Appl. Phys. **115**, 213509 (2014).

[8] P. Reichenbach, T. Kämpfe, A. Thiessen, A. Haußmann, T. Woike, and L. M. Eng, Appl. Phys. Lett. **105**, 122906 (2014).

[9] P. Herth, D. Schaniel, T. Woike, T. Granzow, M. Imlau, and E. Krätzig, Phys. Rev. B **71**, 125128 (2005).

[10] B. Faust, H. Müller, and O. F. Schirmer, Ferroelectrics **153**, 297 (1994).

[11] O. F. Schirmer, M. Imlau, C. Merschjann, and B. Schoke, J. Phys.: Condens. Matter **21**, 123201 (2009).

[12] G. Zatryb, A. Podhorodecki, J. Misiewicz, J. Cardin, and F. Gourbilleau, Nanoscale Res. Lett. **6**, 106 (2011).

[13] D. Berben, K. Buse, S. Wevering, P. Herth, M. Imlau, and T. Woike, J. Appl. Phys. **87**, 1034 (2000).

[14] O. Beyer, D. Maxein, T. Woike, and K. Buse, Appl. Phys. B: Lasers Opt. **83**, 527 (2006).

[15] D. Conradi, C. Merschjann, B. Schoke, M. Imlau, G. Corradi, and K. Polgar, Phys. Status Solidi RRL **2**, 284 (2008).

[16] D. Maxein, S. Kratz, P. Reckenthaeler, J. Bückers, D. Haertle, T. Woike, and K. Buse, Appl. Phys. B: Lasers Opt. **92**, 543 (2008).

[17] C. Merschjann, B. Schoke, D. Conradi, M. Imlau, G. Corradi, and K. Polgar, J. Phys.: Condens. Matter **21**, 015906 (2009).

[18] K. L. Sweeney, L. E. Halliburton, D. A. Bryan, R. R. Rice, R. Gerson, and H. E. Tomaschke, J. Appl. Phys. **57**, 1036 (1985).

[19] Y. Yamada and Y. Kanemitsu, J. Lumin. **133**, 30 (2013).

[20] V. Dierolf, C. Sandmann, S. Kim, V. Gopalan, and K. Polgar, J. Appl. Phys. **93**, 2295 (2003).

[21] V. Dierolf and C. Sandmann, J. Lumin. **125**, 67 (2007).

[22] F. Klose, M. Woehlecke, and S. Kapphan, Ferroelectrics **92**, 181 (1989).

[23] A. Harhira, L. Guilbert, P. Bourson, and H. Rinnert, Phys. Status Solidi C **4**, 926 (2007).

[24] A. Harhira, L. Guilbert, P. Bourson, and H. Rinnert, Appl. Phys. B: Lasers Opt. **92**, 555 (2008).

[25] V. Gopalan and M. C. Gupta, Ferroelectrics **198**, 49 (1997).

[26] C. Merschjann, Ph.D. thesis, Universität Osnabrück, 2007.

[27] H. Xu, A. Chernatynskiy, D. Lee, S. B. Sinnott, V. Gopalan, V. Dierolf, and S. R. Phillpot, Phys. Rev. B **82**, 184109 (2010).

[28] F. Xin, Z. Zhai, X. Wang, Y. Kong, J. Xu, and G. Zhang, Phys. Rev. B **86**, 165132 (2012).

[29] C. Merschjann, M. Imlau, H. Brüning, B. Schoke, and S. Torbrügge, Phys. Rev. B **84**, 052302 (2011).

[30] C. Merschjann, D. Berben, M. Imlau, and M. Wöhlecke, Phys. Rev. Lett. **96**, 186404 (2006).

[31] J. Carnicero, M. Carrascosa, G. García, and F. Agulló-López, Phys. Rev. B **72**, 245108 (2005).

[32] M. Schröder, A. Haußmann, A. Thiessen, E. Soergel, T. Woike, and L. M. Eng, Adv. Funct. Mater. **22**, 3936 (2012).

[33] A. Thiessen, Ph.D. thesis, Technische Universität Dresden, 2013.